Nucleation and Growth in Shock-Induced Phase Transitions and How they Determine Wave Profile Features

Jidong Yu, Wenqiang Wang,* and Qiang Wu

Laboratory for Shock Wave and Detonation Physics, Institute of Fluid Physics, China Academy of Engineering Physics, Mianyang, Sichuan 621900, China

(Received 23 November 2010; published 11 September 2012)

Wave profile measurement and interpretation play a central role in shock physics research. We propose an approach to revealing the direct link between the wave profile and nucleation and growth process in shock-induced phase transition. Through phase field simulations, we show for the first time that it is possible to explain experimentally measured wave profiles directly from the viewpoint of nucleation and growth, and constrain from such profiles real nucleation and growth scenarios that are otherwise impossible to study.

DOI: 10.1103/PhysRevLett.109.115701 PACS numbers: 64.70.K−, 62.50.Ef, 81.30.−t

Introduction.—Despite five decades of studies of phase transitions under shock wave loading [1], the nucleation and growth mechanisms underlying such extremely rapid and complex phenomena are still poorly understood. In particular, where does the product phase nucleate? How fast do the phase boundaries propagate? How do different domains of the product phase interact with one another? And how does this nucleation and growth scenario influence wave propagation? None of these questions have been adequately addressed due to a lack of suitable means of investigation.

On the other hand, wave profile measurement and interpretation play a central role in shock physics research. Theoretically, much information about the dynamic material response can be deduced from a wave profile. However, what information can be obtained solely depends upon how to interpret the wave profile. Conventionally, experimental wave profiles associated with phase transition are simulated and understood by solving a system of equations including the hydrodynamic equations, a constitutive equation, and a phenomenlogical kinetic law [2–4]. The constitutive equation is constructed based on the assumption that a phase transforming material is a mixture of multiple phases. It relates the time variation of pressure and temperature to the variation of mass fractions (of different phases) and density. The kinetic law gives the time rates of change of mass fractions. This approach is useful in the phenomenological explanation of experimental wave profiles and in simulations for engineering applications. However, it cannot reveal from a wave profile any of the microscopic or mesoscopic mechanisms of a phase transition. In this sense, the usefulness of experimental wave profiles as an important window for studying shock-induced phase transition is largely unexplored.

In this Letter, we show that through direct numerical simulation of nucleation and growth, one can clearly reveal the direct link between a wave profile and the nucleation and growth process. In this way, once the simulation reproduces an experimental wave profile, the real nucleation and growth scenario is constrained, and the wave profile is explained. We regard this as a new, mechanism-based approach to studying shock-induced phase transitions.

Equations.—The theoretical basis of our approach is the phase field method, which is a very powerful tool for modeling microstructure evolution [5–11]. It describes a microstructure using a set of order parameters whose temporal evolution is governed by the Allen-Cahn (time-dependent Ginzburg-Landau) equation. We assume the phase transition involves only two phases, which is the case for most phase transitions under shock wave loading. Furthermore, for the reasons discussed in the Supplemental Material [12], we neglect the variants of the product phase that may appear as a higher symmetry phase transforms to a lower symmetry phase (e.g., the martensitic phase transformation in shape memory alloys [13]). Hence, we need only a single order parameter ϕ, with $\phi = 0$, $\phi = 1$, and $0 < \phi < 1$ representing the initial phase, the product phase, and the interface between the two phases, respectively. The Allen-Cahn equation then reads

$$\frac{\partial \phi}{\partial t} = -L\left[\frac{\partial(\rho g)}{\partial \phi} - \beta \nabla^2 \phi\right], \tag{1}$$

where L is the kinetic coefficient, β is the gradient energy coefficient, ρ is the mass density, and g is the specific (per unit mass) Gibbs free energy.

The Gibbs (Helmholtz) free energy is, in general, a function of stress (strain) tensor and temperature. (In the phase field theory it is also a function of order parameter.) However, while it is possible to construct such a function for a thermoelastic material [9–11,14], it is much more difficult to do so for phase transforming solids under shock wave loading. This is because most of these materials plastically yield before changing their phase, which complicates the description of the deviatoric behavior. (For example, both the yield stress and shear modulus may vary with pressure and temperature, and the former may also change with strain

and strain rate.) Because of this complexity, all the existing theoretical works on shock-induced phase transition have included only the volumetric but not the deviatoric contribution in constructing the free energy function [1–4,15,16]. Nevertheless, this is a good approximation for many materials (especially for metals) because their phase transition pressures are far in excess of their yield stresses. We make the same simplification in our approach, so the free energy in Eq. (1) can be written as $g(P, T, \phi)$ where P is pressure and T is temperature. Levitas *et al.* [11] derived a large strain Landau potential that includes the deviatoric contribution and anticipated that it can be easily extended to shock wave problems. This may be true for thermoelastic materials but not for most materials of interest to the shock physics community.

To derive $g(P, T, \phi)$, let us assume that the specific (per unit mass) internal energy e and volume v can be obtained by interpolation between the initial (1) and product (2) phases:

$$e(P, T, \phi) = [1 - h(\phi)]e_1(P, T) + h(\phi)e_2(P, T), \quad (2)$$

$$v(P, T, \phi) = [1 - h(\phi)]v_1(P, T) + h(\phi)v_2(P, T), \quad (3)$$

where $h(\phi) = 3\phi^2 - 2\phi^3$ is the interpolation function. Then, based on these two equations and the thermodynamic relation $de = Tds - Pdv$, one can derive the specific entropy $s = [1 - h(\phi)]s_1 + h(\phi)s_2 + \chi(\phi)$, where $\chi(\phi)$ is an integration constant (see details in the Supplemental Material [12]). Substituting the entropy together with Eqs. (2) and (3) into the thermodynamic relation $g = e - Ts + Pv$, one finally gets

$$g(P, T, \phi) = [1 - h(\phi)]g_1(P, T) + h(\phi)g_2(P, T) + TWf(\phi). \quad (4)$$

Here we have followed Refs. [5–8] to rewrite the term $\chi(\phi)$ in the entropy as $-Wf(\phi)$, so TW is the energy hump between the two phases, and $f(\phi) = \phi^2(1 - \phi)^2$ is a double-well function.

We now derive the phase transition constitutive relation. We still begin with Eqs. (2) and (3). Following Ref. [2], we take time derivatives of these two equations and substitute the adiabatic condition $\dot{e} = -P\dot{v}$ into them to eliminate $\dot{e}$, then we readily obtain the relation between $(\dot{P}, \dot{T})$ and $(\dot{v}, \dot{\phi})$, which is the desired constitutive relation,

$$\begin{pmatrix} \dot{P} \\ \dot{T} \end{pmatrix} = M \begin{pmatrix} \dot{v} \\ \dot{\phi} \end{pmatrix}, \quad (5)$$

where M is a 2×2 matrix whose details are given in the Supplemental Material [12].

Finally, Eqs. (1) and (5) are coupled with the governing equations of hydrodynamics. The wave propagation and nucleation and growth scenario [17] in shock loaded media are simulated by solving these equations with the finite element method [18]. Other important issues, including the spatial-temporal resolution of the simulation; the phase field parameters L, β, and W; and the mesh independence of simulation results, are discussed in the Supplemental Material [12].

Examples.—Some typical examples are given below to show how different nucleation and growth scenarios can lead to different wave profile shapes. The details of the computational models are given in the Supplemental Material [12].

We first qualitatively consider the universal split wave structure with the focus on its transition zone. It is experimentally observed that the slope of this zone can be either negative, zero, or positive. Correspondingly, one sees a loop or a flat or ramped plateau on the wave profile [4,19–21]. A model of shock loaded bismuth is used to study this problem. We find that within some distance from the drive surface, the transition zone of the wave profile always has a negative slope, and this pressure (and particle velocity) decrease is caused by the rarefaction waves emitted from the growing product phase domains (see movies M1, M2 and M3 [12]). The wave profile evolves with propagation distance, and what it will look like at a greater distance is fundamentally determined by the nucleation condition and kinetic coefficient. Figure 1 shows four simulated free surface velocity histories of the shocked Bi sample. Curve A is obtained at sufficiently high kinetic coefficient and nucleation density. It has a perfect split wave structure and has reached the equilibrium state because the phase transition proceeds very rapidly. At moderate kinetic coefficient and nucleation density, one easily obtains a wave profile (curve B) whose transition zone has a negative slope. However, to make that slope positive (curve C) is only possible through reducing the nucleation density gradually along the loading direction. In both cases (i.e., curves B and C), a flat transition zone (curve D) can

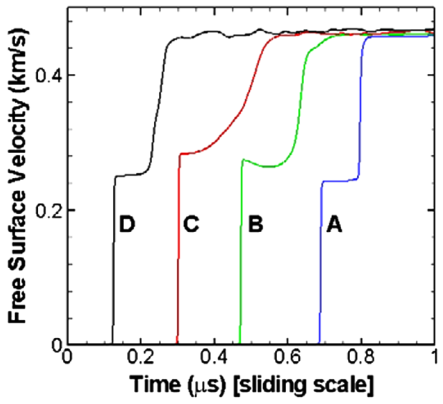

FIG. 1 (color online). Shocked Bi free surface velocity histories. The kinetic coefficients (in $Pa^{-1}s^{-1}$) for curves A, B, C, and D are 3.0, 0.15, 0.15, and 1.0, respectively. The nucleation densities (in μm^{-2}) for A and B are 0.037 and 0.017, respectively. The nucleation distribution is the same for C and D, with the nucleation density gradually decreasing along the loading direction from 0.018 to 0.0007.

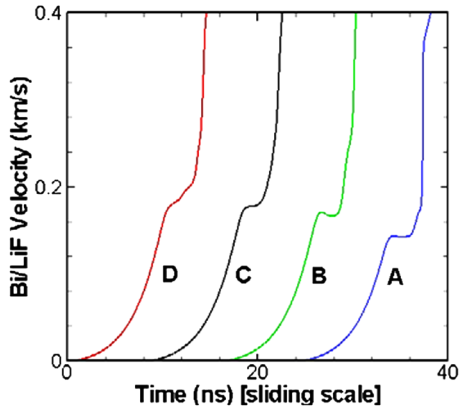

FIG. 2 (color online). Ramp loaded Bi/LiF interface velocity histories. The kinetic coefficients (in $Pa^{-1}s^{-1}$) for curves A, B, C, and D are 125, 12.5, 12.5, and 12.5, respectively. The nucleation densities (in μm^{-2}) are 0.8, 0.08, 0.04, and 0.03, respectively.

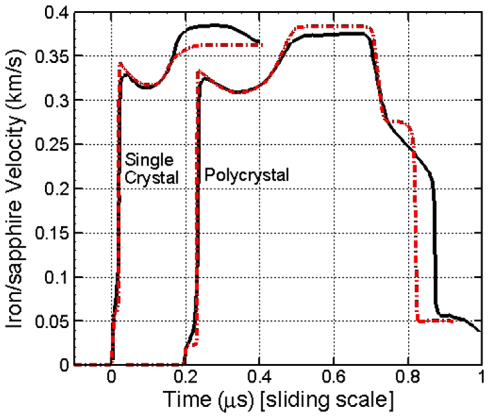

FIG. 3 (color online). Shocked Fe:sapphire interface velocity histories. Red dashed-dotted curves are the simulated results.

be obtained at some higher kinetic coefficient. However, such a plateau is different from the equilibrium state shown in curve A.

The situations under ramp wave loading are similar but simpler. Four simulated wave profiles are shown in Fig. 2. Equilibrium is again reached very rapidly at sufficiently high kinetic coefficient and nucleation density (curve A). Then, with decreasing kinetic coefficient and/or nucleation density, the slope of the transition zone successively becomes negative (B), zero (C), and positive (D). The nucleation density is no longer required to decrease along the loading direction to obtain a ramped transition zone.

We have also quantitatively simulated the recent shock compression experiments on iron [20] and ramp compression experiments on bismuth [21]. Shown in Fig. 3 (corresponding to Fig. 2 in [20]) are the simulated and experimental Fe:sapphire window interface velocities. The corresponding nucleation and growth scenario in polycrystalline iron is shown in movie M4 [12]. Note that curves in Fig. 3 are time shifted for clarity while the time in the movie is the real elapsed time. We find that the α to ε transition must not go to completion to match the experimental wave profiles, and this incomplete transition is not due to the short time scale but is due to an insufficient driving force. This picture is consistent with results from both static and nanosecond shock experiments. For instance, Giles *et al.* [22] estimated that 40% of the α phase was still present at 16.3 GPa in their static high-pressure experiment, Wang *et al.* [23] found that 10% of the α phase still persisted at 18.6 GPa (the highest pressure of their static experiments), while at higher pressures (approximately over 30 GPa) Hawreliak *et al.* [24] observed a complete transformation within a few nanoseconds. (The two-phase region was found to be between 13 and 30 GPa, but unfortunately the fractions of the two phases could not be deduced.) The impact induced peak pressure in our problems is about 16 GPa. For the polycrystal sample, the loading part of the wave profile is well reproduced by randomly forbidding 35.4% of the finite elements to transform (so the ε phase can only nucleate and grow in the other finite elements). However, the simulated release profile associated with the ε to α reverse transition deviates from the experimental one, indicating that the simulated reverse transition proceeds more rapidly. The reason may be complex, and work is under way to improve the model. In the single crystal case, the fraction of the residual α phase is found to be 67.2%. The simulation captures the loop feature of the wave profile. However, the peak velocity is 6% lower than the experimental data, which we think is due to the crystal properties not considered in our model.

For the ramp compression of bismuth, our simulation results are compared with the experimental data in Fig. 4 (corresponding to Fig. 2 in [21]). As an example, the

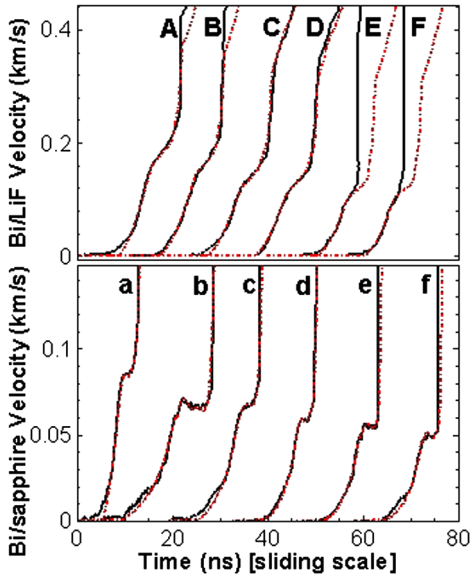

FIG. 4 (color online). Ramp loaded Bi/LiF and Bi:sapphire interface velocity histories. Red dashed-dotted curves are the simulated results.

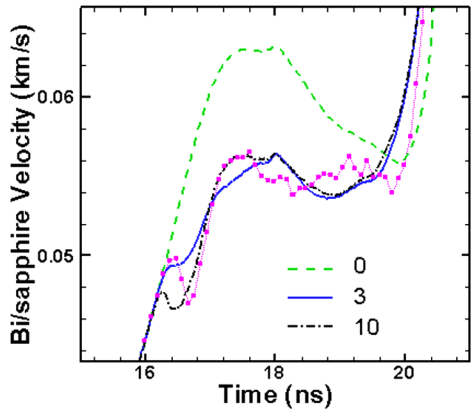

FIG. 5 (color online). Ramp loaded Bi:sapphire interface velocity histories. Numbers indicate the interfacial nucleation densities in μm^{-1}. Purple squares are the experimental data (trace *e* in Fig. 4).

nucleation and growth scenario corresponding to curve *d* is shown in movie M5 [12]. Note that curves in Fig. 4 are time shifted for clarity while the time in the movie is the real elapsed time. All the simulations showed the effect on the wave profile of nucleation at the sample-window interface. In fact, without considering such interfacial nucleation, there is no way to fit the simulated wave profiles to the experimental profiles. This raises a serious question: As measurements are always made at interfaces (including free surface), to what extent does a wave profile reflect the information of the phase transition inside a material? Figure 5 gives an example of how the interfacial nucleation affects the Bi:sapphire interface velocities. The green dashed curve, obtained by assuming no interfacial nucleation, represents the main phase transition signal that originates at the drive surface and evolves through the sample. By comparing this curve with the other two, it can be seen that the interfacial phase transition can reduce the main phase transition signal, and may even produce a small plateau or loop on the wave profile if the interfacial nucleation density is high enough. Note that both the simulated and experimental curves at initial temperatures of 343 and 463 K show these features. When a window with a lower impedance than that of the sample is used (e.g., the Bi/LiF case), its unloading effect hinders the nuclei growth on the sample-window interface, so the signature on the wave profile of the interfacial nucleation is reduced. Such a signature would totally disappear if the measurement was made on free surface.

Summary.—A new, mechanism-based approach has been proposed to better understand shock-induced phase transition. It allows one to explain experimentally measured wave profiles from the viewpoint of nucleation and growth, and more importantly, constrain the real nucleation and growth scenarios that are otherwise impossible to probe. Such inferred scenarios are meaningful at least in the statistical sense and at the coarse grained level.

As is shown in the Supplemental Material [12], both the gradient term and the double-well potential term in Eq. (1) can be dropped at the microscale; therefore, our approach resembles known mixed phase models [2–4]. However, in contrast to these models, our approach describes a discrete microstructure rather than a continuous, smeared distribution of parent and product phases. Also, unlike traditional phase field models, our approach is scale-free because of the absence of the gradient term, and hence, allows for simulations at much larger length and time scales. In this sense, it is similar to the microscale model developed by Levitas *et al.* [9] although the problems and details are different.

Finally, due to the extreme complexity of the problem, our study does not take into account issues such as the mechanism of nucleation (e.g., from dislocations and grain boundaries), anisotropic growth, and martensitic variants and related nanostructures, etc., However, it does take into account the two most important issues (i.e., the spatial distribution of nucleation sites and the propagation of individual phase boundaries.) and can be a good starting point for further research.

We thank R. F. Smith for providing the experimental wave profile data, and L. Truskinovsky for sending his papers on martensitic phase boundaries. This work was supported by the Defence Technology Development Program (A1520070078), the Natural Science Foundation of China (11072228), and the Key Laboratory Science Foundation (9140C6711021007, 9140C6701011101).

Note added.—Recently, we became aware of two papers on the phase field modeling of impact induced phase transformations in shape memory alloys (NiAl and NiTi, respectively). Both have considered martensitic variants. However, in Ref. [25], wave profiles were not studied, and the simulations were on nanoscale which is too small compared with real experiments; Ref. [26] simulated experimental wave profiles with a very coarse finite element mesh (30 μm) obtaining unsatisfactory results. We feel that both works can be improved by considering equations of state specifically developed for the shock loading condition [27,28].

*wwq_mech@hotmail.com

[1] G. E. Duvall and R. A. Graham, Rev. Mod. Phys. **49**, 523 (1977).
[2] D. B. Hayes, J. Appl. Phys. **46**, 3438 (1975).
[3] J. C. Boettger and D. C. Wallace, Phys. Rev. B **55**, 2840 (1997).
[4] P. A. Rigg, C. W. Greeff, M. D. Knudson, G. T. Gray, and R. S. Hixson, J. Appl. Phys. **106**, 123532 (2009).
[5] W. J. Boettinger, J. A. Warren, C. Beckermann, and A. Karma, Annu. Rev. Mater. Res. **32**, 163 (2002).
[6] I. Singer-Loginova and H. M. Singer, Rep. Prog. Phys. **71**, 106501 (2008).
[7] N. Moelans, B. Blanpain, and P. Wollants, CALPHAD: Comput. Coupling Phase Diagrams Thermochem. **32**, 268 (2008).

[8] I. Steinbach, Model. Simul. Mater. Sci. Eng. **17**, 073001 (2009).
[9] V. I. Levitas, A. V. Idesman, and D. L. Preston, Phys. Rev. Lett. **93**, 105701 (2004); A. V. Idesman, V. I. Levitas, D. L. Preston, and J.-Y. Cho, J. Mech. Phys. Solids **53**, 495 (2005).
[10] A. V. Idesman, J. Y. Cho, and V. I. Levitas, Appl. Phys. Lett. **93**, 043102 (2008).
[11] V. I. Levitas, V. A. Levin, K. M. Zingerman, and E. I. Freiman, Phys. Rev. Lett. **103**, 025702 (2009).
[12] See Supplemental Material at http://link.aps.org/supplemental/10.1103/PhysRevLett.109.115701 for movies and theoretical and simulation details.
[13] K. Bhattacharya, *Microstructure of Martensite. Why It Forms and How It Gives Rise to the Shape-Memory Effect* (Oxford University Press, New York, 2004).
[14] V. I. Levitas and D. L. Preston, Phys. Rev. B **66**, 134206 (2002); **66**, 134207 (2002).
[15] C. W. Greeff, D. R. Trinkle, and R. C. Albers, J. Appl. Phys. **90**, 2221 (2001); C. W. Greeff, Model. Simul. Mater. Sci. Eng. **13**, 1015 (2005); L. X. Benedict, T. Ogitsu, A. Trave, C. J. Wu, P. A. Sterne, and E. Schwegler, Phys. Rev. B **79**, 064106 (2009).
[16] J. N. Johnson, D. B. Hayes, and J. R. Asay, J. Phys. Chem. Solids **35**, 501 (1974).
[17] Nucleation in shock loaded materials is mostly heterogeneous and may take place at defects including dislocations, grain boundaries, inclusions, and voids, etc. A critical nucleus may contain only hundreds of atoms. Such physical mechanisms cannot be considered in our approach. However, nucleation can be simulated here by assigning a nonzero initial value (e.g., 0.01) to the order parameters of a certain number of finite element nodes to make them the nucleation sites. In phase field modeling, this is a common way to phenomenologically treat the nucleation problem [9–11]. Although it can not predict the spatiotemporal distribution of nucleation sites from "first principles," it helps infer such information from experimental data (e.g., wave profiles) that are easy to measure.
[18] D. J. Benson, Comput. Methods Appl. Mech. Eng. **99**, 235 (1992).
[19] M. Bastea, S. Bastea, J. A. Emig, P. T. Springer, and D. B. Reisman, Phys. Rev. B **71**, 180101(R) (2005); M. Bastea, S. Bastea, J. E. Reaugh, and D. B. Reisman, Phys. Rev. B **75**, 172104 (2007); M. Bastea, S. Bastea, and R. Becker, Appl. Phys. Lett. **95**, 241911 (2009); D. H. Dolan, M. D. Knudson, C. A. Hall , and C. Deeney, Nature Phys. **3**, 339 (2007).
[20] B. J. Jensen, G. T. Gray, and R. S. Hixson, J. Appl. Phys. **105**, 103502 (2009).
[21] R. F. Smith, J. H. Eggert, M. D. Saculla, A. F. Jankowski, M. Bastea, D. G. Hicks, and G. W. Collins, Phys. Rev. Lett. **101**, 065701 (2008).
[22] P. M. Giles, M. H. Longenbach, and A. R. Marder, J. Appl. Phys. **42**, 4290 (1971).
[23] F. M. Wang and R. Ingalls, Phys. Rev. B **57**, 5647 (1998).
[24] J. A. Hawreliak *et al.*, Phys. Rev. B **83**, 144114 (2011).
[25] J.-Y. Cho, A. V. Idesman, V. I. Levitas, and T. Park, Int. J. Solids Struct. **49**, 1973 (2012).
[26] S.-Y. Yang, J. Escobar, and R. J. Clifton, Mathematics and Mechanics of Solids **14**, 220 (2009).
[27] D. C. Swift, J. G. Niemczura, D. L. Paisley, R. P. Johnson, A. Hauer, R. E. Hackenberg, J. Cooley, D. Thoma, and G. J. Ackland, J. Appl. Phys. **98**, 093512 (2005).
[28] D. C. Swift, D. L. Paisley, K. J. McClellan, and G. J. Ackland, Phys. Rev. B **76**, 134111 (2007).